Icarus 220 (2012) 744–751

Contents lists available at SciVerse ScienceDirect

Icarus

journal homepage: www.elsevier.com/locate/icarus

Modeling specular reflections from hydrocarbon lakes on Titan

Jason M. Soderblom [a,*], Jason W. Barnes [b], Laurence A. Soderblom [c], Robert H. Brown [a], Caitlin A. Griffith [a], Philip D. Nicholson [d], Katrin Stephan [e], Ralf Jaumann [e,f], Christophe Sotin [g,h], Kevin H. Baines [i], Bonnie J. Buratti [g], Roger N. Clark [j]

[a] Lunar and Planetary Laboratory, University of Arizona, Tucson, AZ 85721, USA
[b] Department of Physics, University of Idaho, Moscow, ID 83844, USA
[c] US Geological Survey, Flagstaff, AZ 86001, USA
[d] Department of Astronomy, Cornell University, Ithaca, NY 14853, USA
[e] DLR, Institute of Planetary Research, Berlin, Germany
[f] Department of Earth Sciences, Institute of Geosciences, Free University, Berlin, Germany
[g] Jet Propulsion Laboratory, California Institute of Technology, Pasadena, CA 91109, USA
[h] Université de Nantes, Laboratoire de Planétologie et Géodynamique, Nantes Cedex 03, France
[i] SSEC, University of Wisconsin-Madison, Madison, WI 53706, USA
[j] US Geological Survey, Denver, CO 80225, USA

ARTICLE INFO

Article history:
Received 5 October 2010
Revised 2 May 2012
Accepted 29 May 2012
Available online 7 June 2012

Keywords:
Titan
Saturn, Satellites
Satellites, Surfaces
Satellites, Atmospheres
Infrared observations

ABSTRACT

During the 58th close flyby of Titan (T58), the Cassini Visual and Infrared Mapping Spectrometer (VIMS) observed a specular reflection of sunlight from Titan's Jingpo Lacus through the 5-μm methane window (Stephan, K. et al. [2010]. Geophys. Res. Lett. 37, L07104). The maximum intensity of this reflection is controlled by three basic factors: (1) the shape of the reflecting surface (its overall geometry and roughness), (2) the reflectance of the surface, as controlled by the real refractive index of the material (and that of the atmosphere), and (3) attenuation due to absorption and scattering by atmospheric gases and aerosols along the pathlength. Herein we model the expected intensity of a specular reflection off of a convex mirror-like surface on Titan. We assume the specular reflection is from a body of liquid hydrocarbons on Titan's surface with optical properties consistent with CH_4 and C_2H_6 with smaller amounts of nitrogen and heavier hydrocarbons (e.g., C_3H_8) admixed. We assume the 5-μm opacity for the polar atmosphere is a factor of two higher than that of the tropical haze. For the geometry of the T58 observations, our model predicts a maximum $I/F = 1$-to-5; for a Lambertian surface at normal illumination $I/F = 1$. The maximum 5-μm intensity observed during T58 was $I/F \sim 2.6$, from which we conclude that Jingpo Lacus is filled with a liquid that has a real index of refraction consistent with that of methane–ethane–nitrogen liquid and that the 5-μm atmospheric opacity was $\tau = 0.5$, consistent with the higher particle column expected in the winter polar atmosphere. Future VIMS observations will allow us to refine the refractive index of the liquid in the lakes and to place a quantitative constraint on the ratio of methane to ethane.

© 2012 Elsevier Inc. All rights reserved.

1. Introduction

Observations of Titan have long been searched for specular reflections as evidence of liquid hydrocarbons on the moon's surface (e.g., Muhleman et al., 1990; Griffith et al., 1991; Campbell et al., 2003; Lorenz et al., 2003; Turtle et al., 2005; West et al., 2005). During the 58th close flyby of Titan by Cassini (T58), on 8 July 2009, the first specular reflection of sunlight from Titan's surface was observed at 5 μm (Fig. 1; Stephan et al., 2010) by the Cassini Visual and Infrared Mapping Spectrometer (VIMS; Brown et al., 2004). Stephan and colleagues argued that the observed reflection originated from the surface of Jingpo Lacus, a Cassini RADAR-dark feature located at ~73°N, 335°W, just west of Kraken Mare. Earlier Stofan et al. (2007) had interpreted adjacent features in Cassini SAR (Synthetic Aperture RADAR) data to be examples of the hydrocarbon lakes ubiquitous in the north-polar region.

Observations of specular reflections convey more information about the reflecting surface than simply the presence of liquids. Quantitative analysis of specularly reflected radiation (from a known source, e.g., the Sun or a calibrated source, such as a RADAR) can constrain the physical and compositional properties of a planet's surface and its atmosphere. Wye et al. (2009), for

* Corresponding author. Present address: Department of Earth, Atmospheric and Planetary Sciences, MIT, Cambridge, MA 02139, USA. Fax: +1 617 253 6385.
E-mail address: jms4@mit.edu (J.M. Soderblom).

0019-1035/$ - see front matter © 2012 Elsevier Inc. All rights reserved.
http://dx.doi.org/10.1016/j.icarus.2012.05.030

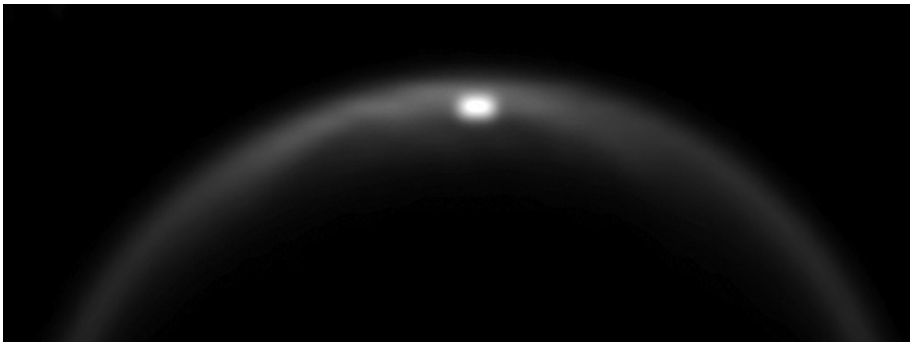

Fig. 1. A 5-μm Cassini VIMS image of the Sun, reflecting from the surface of Jingpo Lacus, a hydrocarbon lake located at ~73°N, 335°W (Stephan et al., 2010). The image has been resampled and smoothed.

example, concluded from observations of a specular return from the Cassini RADAR that the surface of south-polar lake, Ontario Lacus, was extraordinarily smooth at the time of observation. Herein we model the observed intensity of the specular reflection of radiation from a hydrocarbon lake on Titan, both to check its consistency with the expected optical constants of such a hydrocarbon lake, and to constrain the lake's roughness and the scattering properties of the atmosphere.

In this work, we model the absolute intensity of a specular reflection from a smooth planetary surface as a function of range and incidence angle (and equal emission angle), including the effects of the convex shape of the planet's surface, attenuation by the overlying atmosphere, and the magnitude of the surface reflection (controlled by the real parts of the indies of refraction of the reflecting surface and atmosphere). Applying this model to the VIMS T58 observations allows us to constrain the transmission of Titan's atmosphere and the physical character and optical properties (i.e., index of refraction) of the reflecting surface, which in turn provides constraints on the nature and composition of the reflecting surface. Barnes et al. (2010) applied such constraints to model the variations in intensity among the four T58 VIMS observations, limiting wave slopes on Jingpo Lacus to have been <0.05° at the time of T58.

2. Modeling the intensity of the specular reflection

In this paper we model the case of zero roughness (e.g., a wave-free lake, consistent with observations Barnes et al. (2010)) and, in the end, show the very high intensity of the observed reflection to be consistent with a hydrocarbon lake with little or no surface roughness. The maximum observed intensity of a specular reflection from a smooth reflector on a planet's surface is controlled by three basic factors: (1) the geometry of the observation, including the distance from the source to the planet, the distance from the planet to the observer, and the planet's radius, (2) the real index of refraction of the reflecting material (and overlying atmosphere), and (3) scattering and absorption of light within the planet's atmosphere. The intensity of a specular reflection from a planetary surface can be modeled as the product of the intensity of the Sun as viewed through a perfectly reflecting surface (I/F_{Sun}), the surface reflectance ($R_{\text{Surface}}(i,\lambda)$), and the atmospheric transmission ($\text{Atm}(i,\lambda)$):

$$I/F_{\text{Specular}}(i,\lambda) = I/F_{\text{Sun}} \times R_{\text{Surface}}(i,\lambda) \times \text{Atm}(i,\lambda). \quad (1)$$

We present models of each of these terms in the following subsections.

2.1. Intensity of the unresolved Sun

We first derive the expected intensity of an image of the Sun in terms of I/F (where I is the observed radiance and πF is the incident solar flux; defined such that $I/F = 1$ for a perfectly diffuse reflector at normal incidence). In the limit where the Sun is resolved (and limb darkening ignored), the intensity of the Sun can be written as $I_{\text{Sun-Resolved}} = \pi F/\Omega_{\text{Sun}}$, where Ω_{Sun} is the solid angle of the Sun, as seen by the observer. Because both F and Ω_{Sun} scale inversely with the square of the distance from the Sun, $I_{\text{Sun-Resolved}}$ is constant. The I/F of a resolved image of the Sun can, thus, be expressed as

$$I/F_{\text{Sun-Resolved}} = \pi/\Omega_{\text{Sun}}. \quad (2)$$

In the limit where the Sun is unresolved, I/F_{Sun} will scale as the ratio of Ω_{Sun} to the solid angle of the pixel (Ω_{p}) (i.e., the observed solar flux will be averaged over the entire pixel) and can be written as

$$I/F_{\text{Sun}} = \pi/\Omega_{\text{p}}. \quad (3)$$

2.2. Geometric reduction

Equation (3) is valid for both directly viewing the Sun, and viewing the Sun through any number of perfect reflections (including non-planar reflections). In such a case, Ω_{p} is then the solid angle of the pixel projected through the reflection(s). To demonstrate this is valid, consider the intensity of a beam of light before and after any arbitrary reflection. The intensity I of an amount of power P crossing a unit area A, traveling into a solid angle Ω can be written as $I = P/(A \times \Omega)$. The reduction in intensity through the reflection is then, $I_2/I_1 = P_2/(A_2 \times \Omega_2)/\{P_1/(A_1 \times \Omega_1)\}$. Power is conserved if the reflection is perfect and, at a distance sufficiently close to the surface, the cross-sectional area of the two beams is identical. The change in intensity for a perfect reflection from any surface (e.g., a convex mirror) is, therefore, $I_2/I_1 = \Omega_1/\Omega_2$: the ratio of the solid angle of the pixel or IFOV (instantaneous field of view) prior to the reflection to that of the pixel when projected off of the reflecting surface.

The surface of a Titan lake or sea will take the shape of the local gravitational equipotential surface (ignoring external forces). For our purposes, Titan's equipotential surface is closely modeled as a sphere. At a given distance, this convex shape will reduce the observed intensity of a specular reflection relative to a flat surface. This effect is negligible when the observer is very close to the reflecting surface (i.e., a small fraction of the radius of the object), but becomes important far from the surface, as is the case when observing from a spacecraft. A convex mirror causes a collimated beam of light reflected from its surface to diverge, thereby

decreasing the observed intensity relative to that from a plane mirror, or equivalently, directly viewing the object.

To determine the expected intensity for a reflection from planetary surface, we first calculate the solid angle of the pixel, as reflected off the planet's surface. We can approximate the expansion of the IFOV as projected into the down-Sun and cross-Sun directions (Fig. 2). The width of the IFOV projected onto the convex surface in the down-Sun direction (which lies in the Sun-specular-VIMS plane) is approximately $L_{\text{down-Sun}} \sim D \times \text{IFOV}/\mu_o$, where D is the distance from the observer to the surface and μ_o is the cosine of the incidence angle (also emission angle) for the central ray (Sun-surface-observer). Assuming the IFOV is small compared to the IFOV projected down-Sun ($\text{IFOV}^*_{\text{down-Sun}}$), this can be written as:

$$\text{IFOV}^*_{\text{down-Sun}} \sim 2D \times \text{IFOV}/(r \times \mu_o), \tag{4}$$

where r is the planetary radius. The width of the IFOV projected onto the convex surface in the cross-Sun direction can be approximated as $L_{\text{cross-Sun}} \sim D \times \text{IFOV}$. Again, assuming the IFOV is small compared to the IFOV projected cross-Sun ($\text{IFOV}^*_{\text{cross-Sun}}$), this can be written as:

$$\text{IFOV}^*_{\text{cross-Sun}} \sim 2D \times \mu_o \times \text{IFOV}/r. \tag{5}$$

The expanded solid angle, projected off of the convex surface into the sky (Ω^*_p) can then be approximated as; $\Omega^*_p = (\text{IFOV}^*_{\text{down-Sun}} \times \text{IFOV}^*_{\text{cross-Sun}})$. Substituting the approximations given in Eqs. (4) and (5), Ω^*_p can be written in terms of the solid angle of a pixel at the instrument, $\Omega_i = \text{IFOV}^2$, as:

$$\Omega^*_p \sim \Omega_i(2D/r)^2, \text{ or } \Omega_i/\Omega^*_p \sim [r/(2D)]^2. \tag{6}$$

This approximation for Ω^*_p can be then be substituted into Eq. (3) to estimate the I/F of the Sun viewed through the reflection off of a convex surface.

Equation (6) is only an approximation but illustrates the functional dependence of the geometric reduction in intensity on distances and angles and is useful in planning future observations. The approximation suggests the reduction in intensity is independent of incidence angle and scales with the inverse square of the distance from the planet to the spacecraft. This approximation is valid for all wavelengths, including UV and RADAR wavelengths, so long as the source is unresolved and the projected IFOV is large compared to the instrument IFOV—generally true for distances greater than several planetary radii. (Viewed directly, the Sun's angular diameter is roughly twice the VIMS IFOV when operating in nominal mode.) Furthermore, the projected IFOV becomes quite distorted at large range and high incidence angles. Iterative numerical calculations via ray tracing provide a more accurate estimate of the geometric effect and are more suitable for precisely modeling the intensity of such observations.

Fig. 3 illustrates results of such numerical calculations for a spacecraft distance of 100 planetary radii (similar to the T58 observations). Equation (6) gives an estimate $\Omega_i/\Omega^*_p \sim 2.50 \times 10^{-5}$ for this case. The numerical estimates are quite close to this value (given in left-hand frames in Fig. 3) and illustrate that the intensity reduction *is*, in fact, largely independent of incidence angle. This holds true at incidence angles as large as 75° ($\Omega_i/\Omega^*_p \sim 2.45 \times 10^{-5}$), even as the projected IFOV (left pane), specular footprint of the Sun on the planetary surface (center pane), and Sun projected into the instrument IFOV (right pane) become highly distorted. Two methods to estimate Ω_i/Ω^*_p give the same result: the first is the ratio of the solid angles of the instrument IFOV and that of the IFOV projected around the Sun (left panes); the second is the ratio of the solid angle of the Sun projected into the instrument IFOV (right panes) to that of the Sun viewed directly. Table 1 extends this comparison over the practical range of VIMS specular observations that can be acquired (from distances of 10, 100, and 1000 Titan radii); the simple approximation diverges from the numerical results by only 10–20%.

Zero-phase cases ($i = \varepsilon = 0°$) provide an additional opportunity to explore the geometric behavior (Fig. 4). In these cases an analytical solution for the width and height of the projected IFOV is trivial. An estimate of Ω_i/Ω^*_p from this solution is shown by the solid curve in Fig. 4. Below ~10 planetary radii, where the analytical solution rapidly diverges from the approximation, the analytical solution approaches $\Omega_i/\Omega^*_p \sim 1$ as the S/C-surface distance approaches zero, as one expects as the mirror surface approaches a flat plane.

It is noteworthy that, contrary to natural intuition, for cases at high altitude and high incidence angle, the footprint of the Sun's specular reflection on a planet's surface is heavily foreshortened in the down-Sun direction (illustrated in Fig. 3). The reason for this apparent paradox is that the effects of the reflection from a convex surface can, for certain geometries, produce a larger effect than the commonly observed effects of elongating a reflection in the down-range direction for a flat surface. It is important to thoroughly understand this effect, as it controls the surface that is sampled in a specular reflection observation.

2.3. Reflection from a hydrocarbon lake

A hydrocarbon lake is not a perfect reflector. Because it is a dielectric, with a real index of refraction is greater than 1, only a fraction of the incident light is specularly reflected from the lake surface. The power reflected from such a surface depends on the refractive indices of the surface and overlying atmosphere, as well as the incidence angle and polarization of the incident radiation. For Titan, the refractive index of the atmosphere is very close to 1 in the infrared, and the light can be assumed to be randomly polarized. Reflection coefficients calculated using the Fresnel Equations (e.g., Hecht, 1998) are plotted in Fig. 5 as functions of incidence angle and index of refraction. Atmospheric refraction potentially has a second effect of altering the angle of incidence

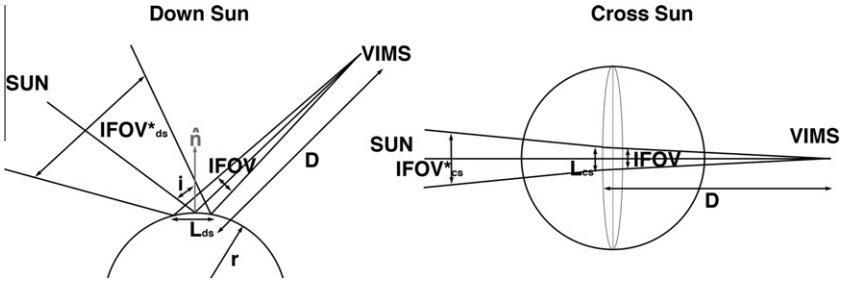

Fig. 2. Cartoons showing expansion of the VIMS IFOV reflected from a convex surface. Left: the down-Sun (i.e., the Sun-Titan-VIMS plane) direction; right: cross-Sun direction.

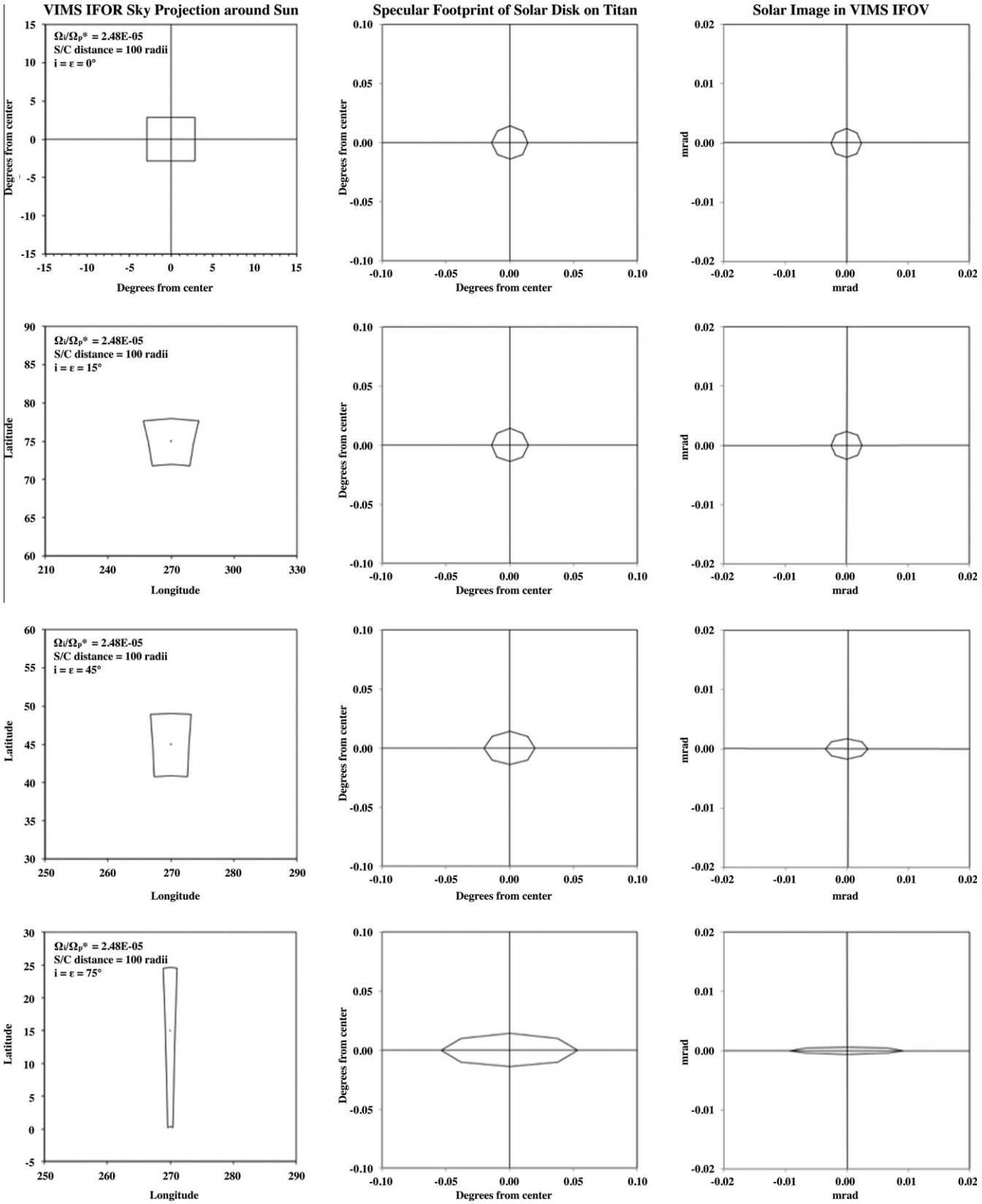

Fig. 3. Numerical calculations of the geometric effects for VIMS viewing a specular reflection of the Sun from a spacecraft-surface distance of 100 planetary radii (100 *r*) for incidence angles (and therefore emission angles) of 0°, 15°, 45° and 75°. Left: the VIMS IFOV projected from the instrument off of the convex mirror surface into the sky around the Sun (the top left pane is plotted in angle from a polar center); middle: specular footprint of the Sun plotted on Titan's surface (again, plotted in angle from a polar center); right: image of the Sun plotted within the VIMS IFOV.

Table 1
Comparison of approximation and numerical solutions for Ω_i/Ω_p^*.

Surface-S/C dist. (in planetary radii)	Approximation $\Omega_i/\Omega_p^* \sim [r/(2D)]^2$	Numerical solutions for Ω_i/Ω_p^*			
		$i = \varepsilon = 0°$	$i = \varepsilon = 15°$	$i = \varepsilon = 45°$	$i = \varepsilon = 75°$
1000 r	2.50×10^{-07}	2.50×10^{-07}	2.50×10^{-07}	2.50×10^{-07}	2.49×10^{-07}
100 r	2.50×10^{-05}	2.48×10^{-05}	2.48×10^{-05}	2.47×10^{-05}	2.45×10^{-05}
10 r	2.50×10^{-03}	2.27×10^{-03}	2.27×10^{-03}	2.25×10^{-03}	2.07×10^{-03}

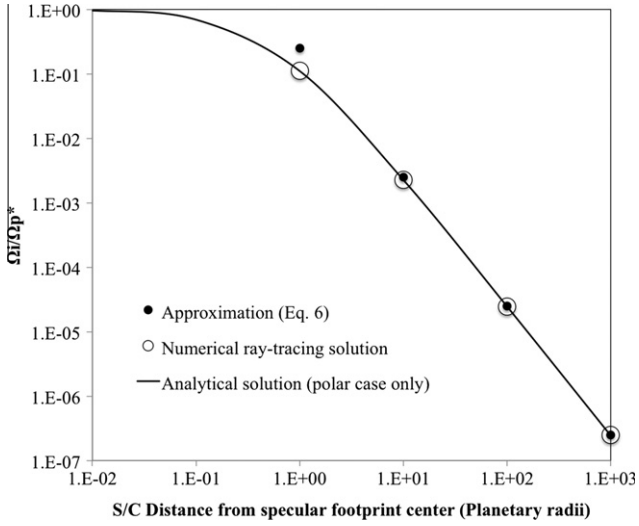

Fig. 4. Comparison of three estimates for zero-phase cases ($i = \varepsilon = 0°$). The solid curve plots an estimate for Ω_i/Ω_p^* from an analytical solution for the width and height of the projected IFOV around the Sun. Notice that the solution approaches unity as the S/C-surface distance approaches zero.

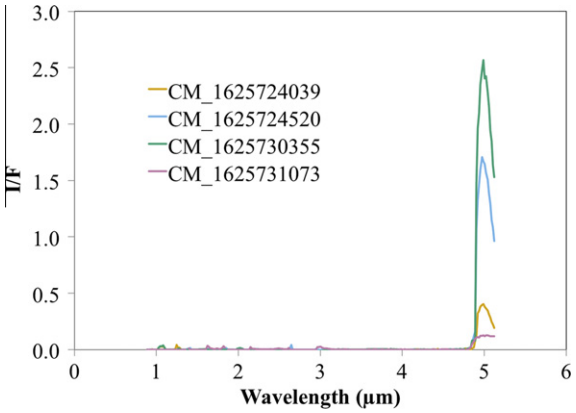

Fig. 6. Spectra of solar radiation specularly reflected from the surface of Titan acquired by VIMS on T58. Data are from the single brightest pixel from each observation. Radiation that is not specularly reflected from Titan's surface was removed by subtracting an average of the pixels surrounding the specular reflection, normalized at 4 μm. Scattering and absorption by Titan's atmosphere obscures the specular reflection shortward of the 5-μm window (Stephan et al., 2010).

of the ray at the surface. This effect can be shown to be negligible for Titan, resulting in a change in the incidence angle from the top of the atmosphere to the bottom of ~0.1° (for a conventional N_2–CH_4 Titan atmosphere with a scale height of 40 km) and can be ignored (P.J. Gierasch, private communication).

2.4. Atmospheric scattering and absorption

The VIMS specular reflection reported by Stephan et al. (2010) was only observed in the 5-μm atmospheric transmission window and undetectable at shorter wavelengths (Fig. 6). Specular reflections are manifested in the direct beam by incoming and outgoing photons that are unscattered by the atmosphere. Scattering by aerosols in Titan's atmosphere reduces the fraction of direct flux that reaches the surface, scattering being increasingly stronger at shorter wavelengths (Bellucci et al., 2009). For large incidence and emission angles, and therefore long pathlengths (e.g., the T58 specular-reflection observations where $i = \varepsilon \sim 73°$), this results in a complete obscuration of VIMS-observed specular signals shortward of the 5-μm window (Stephan et al., 2010).

To quantitatively estimate the atmospheric attenuation, $\mathrm{Atm}(i, \lambda)$, of the direct beam reaching the surface and of the outgoing specular reflection, we start with the atmospheric radiative transfer model published by Griffith et al. (2012) for the equatorial region at the Huygens landing site. That model uses the discrete

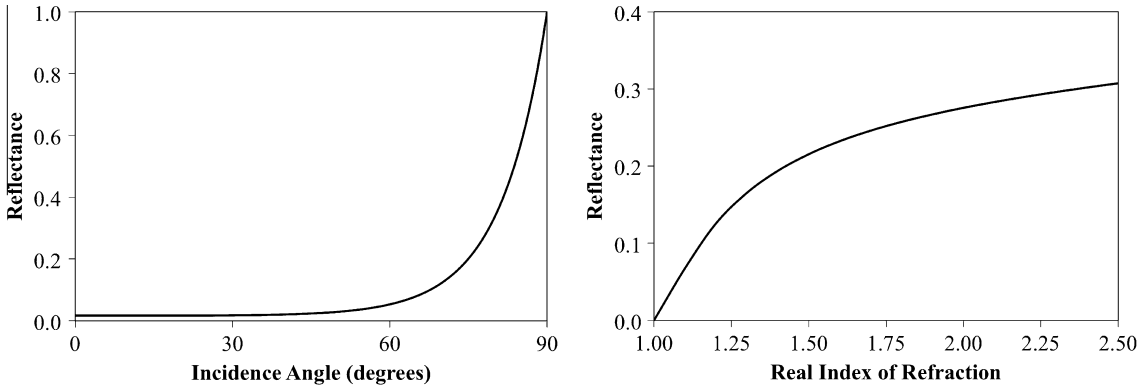

Fig. 5. Total reflectance, calculated from the Fresnel reflection coefficients plotted on the left as a function of incidence angle for a real index of refraction of 1.3 (a reasonable assumption for the refractive index at 5 μm of Titan's lakes), and on the right as a function of the real index of refraction for an incidence angle of 73° (the geometry of the T58 observation shown in Fig. 1).

ordinates radiative transfer approximation of Stamnes et al. (1988) with a 70-layer plane-parallel atmosphere. Results are shown to be in excellent agreement with doubling and adding radiative transfer calculations long used by Tomasko and colleagues (cf. Tomasko et al., 2005) in analyzing Huygens Descent Imager/Spectral Radiometer (DISR) measurements. Optical properties of the aerosol haze used in the Griffith et al. model are those of Tomasko et al. (2008b), who derived them using DISR measurements from 0.35 μm to 1.6 μm, extrapolated to 5 μm with fractal models of aerosol particles. The methane opacity parameters shortward of 1.6 μm are taken from Tomasko et al. (2008a) and slightly modified based on work of de Bergh et al. (2012), while methane opacity longward of 1.6 μm and that of carbon monoxide are calculated using HITRAN line parameters (Rothman et al., 2008).

The equatorial atmosphere above Huygens landing site ~10°S, is quite dry, whereas the winter polar atmosphere is dominated by methane and ethane condensates (cf. Rannou et al., 2006; Griffith et al., 2006). The higher particle column expected in the winter polar atmosphere will result in an opacity that is significantly higher than that of the tropical regions. Griffith et al. (2012) estimate the haze optical depth at 4.8 μm at the Huygens landing site to be 0.2-to-0.3. We assume the 5-μm particle opacity for the polar regions is a factor of two higher than that reported by Griffith et al. for the tropical regions and show this to be consistent with the observed specular intensity.

It should be noted that uncertainties in extrapolating the scattering properties of the aerosols derived from the Huygens data first to 5 μm and then to high polar latitudes, leads to significant uncertainties in the haze optical depth in modeling the polar specular reflections. For the geometry of the T58 observations, the modeled attenuation is likely accurate to only within a factor of two or so. As we discuss in Section 3.3, herein we are able to invert the problem and use the T58 VIMS observations to better constrain the atmospheric attenuation in the polar region.

3. Application to VIMS T58 specular reflection observations

The specular reflection (Fig. 1) reported by Stephan et al. (2010) was observed in four separate VIMS observations spanning a period of ~2.5 h acquired during the T58 flyby (cf. Fig. 6). These data were acquired as part of a cloud-monitoring sequence that targeted Titan's limb during flyby ingress. The phase angles of these observations ranged from 146.3 to 146.6° and the spacecraft altitude ranged from ~234,000 to 194,000 km (yielding image scales of 97–117 km/pixel).

3.1. Reconstructed geometry of the T58 specular reflection

Using navigation solutions for the positions of the Cassini spacecraft and the Sun in a Titan-body-centered coordinate frame, the geometry of the four T58 VIMS observations can be reconstructed with a precision of ~1 km. Cassini SPICE (Spacecraft-position, Planet-definition, Instrument, Camera-pointing, and Events) kernels provide data to compute the light-time corrected coordinates of the Sun and the Cassini spacecraft in a Titan-body-centered system using tools provided by JPL's Navigation and Ancillary Information Facility (NAIF). Proper reconstruction of the geometry at the specular reflection (incidence or emission, phase angles), however, necessitates first solving for the location of the specular point on Titan's surface, which is offset from the center by Titan's radius. Refraction in Titan's atmosphere is ~0.1° for the given geometry has negligible effect on the results and is not included in our model.

The reconstructed geometries of the T58 specular reflections are shown in Fig. 7. The second and third observations appear to fall most completely within Jingpo Lacus and correspond to the brightest reflections (cf. Fig. 6). The brightest reflection, which occurred in the third observation, had an incidence angle of 73.25° and a spacecraft altitude (measured to the sub-spacecraft point) of 198,300 km.

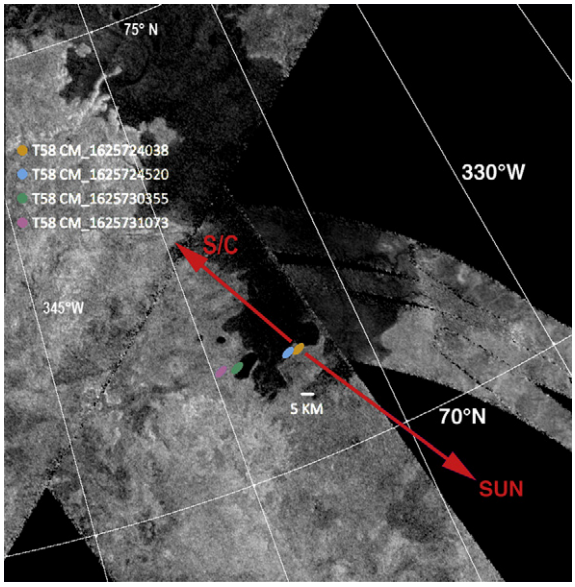

Fig. 7. Location and shape of the solar footprint for the T58 specular-reflection observations mapped onto a RADAR SAR base map. The elongation of the solar footprint in the cross-Sun direction (cf. Section 2.2) is evident in this figure.

3.2. Maximum intensity for the T58 specular reflection

Using estimates for each component in Eq. (1), we can predict the maximum expected intensity of a specular reflection for the specific geometry of the T58 specular-reflection observations. Employing the numerical approach described in Section 2.2, with an instrument IFOV = 0.5 mrad (Brown et al., 2004) and a planet radius of ~2575 km, we estimate the solid angle of the VIMS pixel as projected from Titan's surface for the T58 geometry, $\Omega_p^* \sim 4.19 \times 10^{-3}$ sr. Substituting this into Eq. (3), yields I/F_{Sun} = 488 for a perfectly reflecting convex surface observed with the T58 geometry (~10^4 lower than would be observed when viewing the Sun though a perfectly reflecting flat surface).

Next we assume a lake composed of liquid hydrocarbons, primarily methane and ethane, with a small amount of nitrogen (cf. Lunine et al., 1983; Brown et al., 2008). A reasonable assumption for the real index of refraction at 5 μm of such a liquid is ~1.3 (cf. Badoz et al., 1992; Martonchik and Orton, 1994; Clark et al., 2009). A lake composed primarily of ethane and nitrogen would have an index of refraction closer to 1.4, while a lake composed primarily of methane and nitrogen would have an index of refraction just below 1.3 (cf. Badoz et al., 1992; Clark et al., 2009). Fig. 5 shows Fresnel amplitude reflection coefficients for a methane–ethane–nitrogen liquid surface, plotted as a function of incidence angle. For the geometry of the third T58 observation, we estimate $R_{Surface}$ = 0.165 at 5 μm (assuming the 5-μm index refractive of Titan's atmosphere at the surface = 1). Assuming that the lake is composed of ethane and nitrogen would only increase the observed reflectance by less than 20%, while assuming the lake is composed of only methane and nitrogen would decrease the observed reflectance by only a few percent (at high incidence angles, the Fresnel coefficients are less sensitive to the refractive

index of the surface – implications of this are discussed further in Section 3.3 and the Addendum).

We use the model described in Section 2.4 to estimate attenuation by Titan's atmosphere of the T58 observations. For an incidence/emission angle of 73.25° this model predicts a total attenuation along the two-way path of 5-μm radiation reflected off of the lake to ~0.015–0.063. At 2 μm, the second-clearest window accessible to VIMS, only $\sim 4 \times 10^{-5}$ of the direct flux survives the two-way path through Titan's atmosphere at this incidence angle.

Incorporating these results into Eq. (1), we predict the maximum I/F for a specular reflection entirely from a smooth hydrocarbon lake on Titan's surface, with the geometry of the T58 observations to be $I/F_{\text{specular}} \sim$ 1-to-5 at 5 μm. At 2 μm, we predict the intensity to be three orders of magnitude less ($I/F_{\text{specular}} \sim 0.004$): on order a few percent of the flux diffusely scattered from the surface at this wavelength (assuming the real index of refraction of the liquid surface at 2 μm is ~1.3 (cf. Badoz et al., 1992; Martonchik and Orton, 1994; Clark et al., 2009) and that of the atmosphere is 1). VIMS has inadequate SNR, and the variability of the magnitude of the diffusely scattered light is too large to detect a specular reflection at 2-μm for the T58 observation.

3.3. Constraining atmospheric transmission at 5 μm

As noted in Section 2.4, uncertainties in the scattering properties, column abundance, and distribution of aerosols lead to significant systematic errors in the models used to constrain the fraction of flux attenuated by Titan's atmosphere at 5 μm and particularly at high polar latitudes. If we invert the problem, however, we can use these results to constrain the polar haze opacity and place an upper limit on its value. If we assume that the lake is in fact filled with a mixture of hydrocarbons that has a real index of refraction of 1.3 at 5 μm, then we can use Eq. (1) to solve for the attenuation of 5-μm radiation by Titan's atmosphere. The nature of the T58 VIMS specular reflection observation (i.e., the high incidence angle) makes it ideal for this exercise. High incidence angles result in longer pathlengths, making the observed intensity more sensitive to atmospheric attenuation. Furthermore, the Fresnel coefficients become increasingly insensitive to the refractive index of the surface material at higher incidence angle. The maximum observed intensity of the T58 specular reflection observations was $I/F \sim 2.6$ at 5 μm (cf. Fig. 6). Using this value in our model (with a Fresnel reflection coefficient of 0.165), we conclude that for this observation, ~0.18 of the incident 5-μm radiation reached the surface as direct flux. This equates to a polar haze optical depth of $\tau = 0.5$, roughly two times that of the tropical region estimated by Griffith et al. (2012) from the Huygens data; a higher polar haze opacity is consistent with expectations from other studies (Rannou et al., 2006; Griffith et al., 2006).

4. Discussion: specular reflection from a liquid vs. a solid surface

A specular reflection by itself does not necessarily require a surface liquid. Could the surface at the site of the specular reflections be a solid surface? Although a polished solid surface that is mirror-like at 5 μm and expands for many 10's of km is a highly improbable construction, expanses of granular solids that exhibit strong forward scattering do produce specular glints. Here we address the question as to whether such a surface could account for the intensity of the specular reflection observed during the T58 flyby.

A 100% diffusely reflecting surface (i.e., Lambertian) at an incidence angle of 73° would exhibit an $I/F \sim 0.3$ in the absence of an atmosphere. The minimum two-way 5-μm attenuation presented in Section 3.2 for this geometry (~0.063) would reduce this I/F to ~0.02. Estimates of the 5-μm albedo for the brightest areas observed by VIMS (Tui and Hotei Regio) are ~0.1–0.2 (Soderblom et al., 2009). Using the larger value reduces the observable I/F to ~0.004. Finally, if we assume an extreme case in which the forward scattering lobe is 50× the intensity of the diffuse component, the specular glint from our hypothetical granular forward-scattering surface would yield an I/F of only ~0.2 which is an order of magnitude less than the $I/F \sim 2.6$ observed on T58. We suggest that producing the observed high intensity of the specular reflection with a solid surface is a highly improbable proposition, requiring an unrealistic combination of both unusually high forward scattering and extremely high 5-μm albedo that has nowhere yet been observed on Titan. We conclude that a liquid hydrocarbon lake is the far more probable scenario.

5. Summary

We have presented a model of the maximum intensity expected from the specular reflection of 5-μm solar radiation from a hydrocarbon lake on Titan's surface and have used this model to estimate the intensity of the specular reflection of sunlight from Jingpo Lacus, Titan, as reported by Stephan et al. (2010). For the geometry of these observations, we estimate peak I/F = 1-to-5. The intensity of the specular reflection reported by Stephan et al. (2010) varied significantly between observations (cf. Fig. 6) as the projection of the solar disk moved between lake and non-lake surfaces (Barnes et al., 2010). For the purposes of this work we are only concerned with the maximum observed brightness, which occurred in the third observation, with $I/F \sim 2.6$ at 5 μm (cf. Fig. 6).

We therefore conclude that the specular reflection observed by VIMS on T58 reported by Stephan et al. (2010) is in fact due to light reflected from a liquid surface on Titan. Further, if we assume a real index of refraction for the lake of 1.3, consistent with hydrocarbons such as methane and ethane (cf. Badoz et al., 1992; Martonchik and Orton, 1994; Clark et al., 2009), we are able to constrain the transparency of Titan's polar atmosphere at 5 μm. We estimate from our model of a hydrocarbon lake with an index of refraction of 1.3 that, at the time and for the geometry of this observation (Ls ~359°, latitude ~75°N, i ~73°), ~0.18 of the 5-μm radiation incident on Titan's atmosphere reached the surface as direct flux. This equates to a normal optical depth of $\tau = 0.5$ at 5 μm, ~2 times greater than the opacity modeled for the equatorial atmosphere at the Huygens landing site by Griffith et al. (2012). Effects not considered in this work, such as clouds and waves, and the possibility that only part of the specular image of the Sun is on the lake at the time of the observation, all will have the effect of decreasing the total power and would require less power be removed by the atmosphere to match the observed flux, thus making this an upper limit on the optical depth.

6. Addendum: future observations

The refractive indices of liquid methane and liquid ethane (with and without dissolved nitrogen) differ by ~0.1 at Titan's surface temperature and pressure (cf. Badoz et al., 1992). With subsequent VIMS observations of specular reflections, it should be possible to provide tight enough constraint on the index of refraction of the liquid to determine if a lake's composition is predominately methane or ethane. As we discussed in Section 3.3, at high incidence angles, the Fresnel coefficients are relatively insensitive to the refractive index of the surface material, while atmospheric effects are more pronounced. The opposite is true at low incidence angles, where the power reflected from the surface depends more strongly on the refractive index of the surface material and less on atmospheric effects. This is demonstrated in Fig. 8, in which three

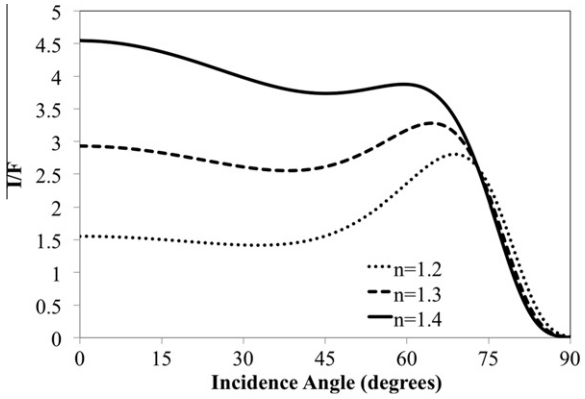

Fig. 8. Models of the intensity of a specular reflection plotted as a function of i, for three different indices of refraction. In each model, atmospheric attenuation is scaled so that the modeled intensity matches the T58 VIMS observation (i.e., $I/F = 2.6$ at $i = 73°$). Note the solutions are quite similar at higher incidence angles but diverge significantly at lower incidence angles.

models of the intensity of a specular reflection are plotted as a function of incidence angle, for three different indices of refraction: 1.2, 1.3, and 1.4. In each model, atmospheric attenuation is scaled so that the modeled intensity match that observed in the T58 VIMS observations (i.e., $I/F = 2.6$ at $i = 73°$). Fig. 8 demonstrates that, for higher incidence angles, the model results are very similar (i.e., at $i > 73°$ the models do not diverge significantly), while at lower incidence angles the three models do diverge significantly.

Acquiring an observation of a specular reflection of the Sun at the lowest incidence angle possible will afford the best opportunity to constrain the real index of refraction of a Titan lake using the methods described in this paper. On Titan, because the lakes are constrained to the polar regions, the observing geometries are somewhat limited. The lowest incidence angles will be achieved around the time of Northern summer, when the Sun will be high in the Northern sky; at Summer Solstice (which next occurs in 2017), the minimum incidence angle at the largest mare will be ~40°. We therefore recommend repeating this observation late in the Cassini Mission, as near to the Summer Solstice, as near to local noon, and on a lake as low in latitude as possible.

In order for a specular reflection of sunlight to be apparent at wavelengths shorter than 5 μm, we must design an observation in which less power is lost as a result of the effects described in Section 2. The two free parameters that we will consider are the incidence angle and the spacecraft altitude. Decreasing the spacecraft altitude will result in an increase in observed intensity, as less power being is lost due to the geometric defocusing of the reflected sunlight (see Section 2.2). Decreasing the incidence angle, however, results in competing effects: a decrease in total atmospheric pathlength resulting in less atmospheric scattering and therefore an increase in intensity, but a decrease in the total power reflected at the surface resulting in a decrease in intensity (see Fig. 5). The dependence of intensity on incidence angle is shown in Fig. 8. A local maximum in intensity is expected at an incidence angle of ~60–70°, depending on the refractive index of the surface. A second maximum in intensity is expected as the incident light approach normal incidence. On Titan, however, this geometry is not accessible for the current distribution of the lakes on Titan. Taking this into consideration, an ideal geometry to observe a specular reflection at 2 μm on Titan, therefore, will be at low altitude and an incidence angle of ~60–70°. At an altitude of ~25,000 km and an incidence angle of 65° the flux of a specular reflection at 2 μm will be on order the same as the 2-μm flux diffusely scattered from Titan and should be apparent to the observer.

Acknowledgments

We wish to thank to the VIMS operations group as well as the entire Cassini project for their tremendous efforts delivering Cassini to Saturn and obtaining and returning these data. We thank Peter Gierasch for providing calculations of refraction in Titan's atmosphere. We thank Ralph Lorenz and an anonymous reviewer for their helpful review of this manuscript. This work was supported by the Cassini Project, managed by the Jet Propulsion Laboratory, California Institute of Technology and under contract with NASA.

References

Badoz, J., Le Liboux, M., Nahoum, R., Israel, G., Raulin, F., Torre, J.P., 1992. A sensitive cryogenic refractometer. Application to the refractive index determination of pure or mixed liquid methane, ethane, and nitrogen. Rev. Sci. Instrum. 63, 2967–2973.

Barnes, J.W. et al., 2010. Wave constraints for Titan's Jingpo Lacus and Kraken Mare from VIMS specular refection lightcurves. Icarus 211, 722–731.

Bellucci, A. et al., 2009. Titan solar occultation observed by Cassini/VIMS: Gas absorption and constraints on aerosol composition. Icarus 201, 198–216.

Brown, R.H. et al., 2004. The Cassini Visual and Infrared Mapping Spectrometer (VIMS) investigation. Space Sci. Rev. 115, 111–168.

Brown, R.H. et al., 2008. The identification of liquid ethane in Titan's Ontario Lacus. Nature 454, 607–610.

Campbell, D.B., Black, G.J., Carter, L.M., Ostro, S.J., 2003. Radar evidence for liquid surfaces on Titan. Science 302, 431–434.

Clark, R.N., Curchin, J.M., Hoefen, T.M., Swayze, G.A., 2009. Reflectance spectroscopy of organic compounds. I: Alkanes. J. Geophys. Res. 114, E03001.

de Bergh, C. et al., 2012. Applications of a new set of methane line parameters to the modeling of Titan's spectrum in the 1.58 micron window. Planet. Space Sci. 61, 85–98.

Griffith, C.A., Owen, T., Wagener, R., 1991. Titan's surface and troposphere, investigated with ground-based, near-infrared observations. Icarus 93, 362–378.

Griffith, C.A. et al., 2006. Evidence for a polar ethane cloud on Titan. Science 313, 1620–1622.

Griffith, C.A., Doose, L., Tomasko, M.G., Penteado, P.F., See, C., 2012. Radiative transfer analyses of Titan's tropical atmosphere. Icarus 218, 975–988.

Hecht, E., 1998. Optics, third ed. Addison Wesley Longman, Inc., Berlin, ISBN 0-201-83887-7.

Lorenz, R.D., Biolluz, G., Encrenaz, P., Janssen, M.A., West, R.D., Muhleman, D.O., 2003. Cassini RADAR: Prospects for Titan surface investigations using the microwave radiometer. Planet. Space Sci. 51, 353–364.

Lunine, J.I., Stevenson, D.J., Yung, Y.L., 1983. Ethane ocean on Titan. Science 222, 1229–1230.

Martonchik, J.V., Orton, G.S., 1994. Optical constants of liquid and solid methane. Appl. Opt. 33, 8306–8317.

Muhleman, D.O., Grossman, A.W., Butler, B.J., Slade, M.A., 1990. Radar reflectivity of Titan. Science 25, 975–980.

Rannou, P., Montmessin, F., Hourdin, F., Lebonnois, S., 2006. The latitudinal distribution of clouds on Titan. Science 311, 201–205.

Rothman, L.S. et al., 2008. The *HITRAN* 2008 molecular spectroscopic database. J. Quant. Spectrosc. Radiat. Transfer 110, 533–572.

Soderblom, L.A. et al., 2009. The geology of Hotei Regio, Titan: Correlation of Cassini VIMS and RADAR. Icarus 204, 610–618.

Stamnes, K., Tsay, S.-C., Wiscombe, W., Jayaweera, K., 1988. Numerically stable algorithm for discrete-ordinate-method radiative transfer in multiple scattering and emitting media. Appl. Opt. 27, 2502–2509.

Stephan, K. et al., 2010. Specular reflection on Titan: Liquids in the Kraken Mare. Geophys. Res. Lett. 37, L07104.

Stofan, E.R. et al., 2007. The lakes of Titan. Nature 445, 61–64.

Tomasko, M.G. et al., 2005. Rain, winds and haze during the Huygens probe's descent to Titan's surface. Nature 438, 765–778.

Tomasko, M.G., Bézard, B., Doose, L., Engel, S., Karkoschka, E., 2008a. Measurements of methane absorption by the Descent Imager/Spectral Radiometer (DISR) during its descent through Titan's atmosphere. Planet. Space Sci. 56, 624–647.

Tomasko, M.G. et al., 2008b. A model of Titan's aerosols based on measurements made inside the atmosphere. Planet. Space Sci. 56, 669–707.

Turtle, E.P. et al., 2005. Liquid hydrocarbons on Titan's surface? How Cassini ISS observations fit into the story (So Far). Lunar. Planet. Sci. XXXVI, 2311 (abstract).

West, R.A., Brown, M.E., Salinas, S.V., Bouchez, A.H., Roe, H.G., 2005. No oceans on Titan from the absence of a near-infrared specular reflection. Nature 436, 670–672.

Wye, L.C., Zebker, H.A., Lorenz, R.D., 2009. Smoothness of Titan's Ontario Lacus: Constraints from Cassini RADAR specular reflection data. Geophys. Res. Lett. 36, L16201.